European Journal of Nuclear Medicine and Molecular Imaging (2020) 47:355–365
https://doi.org/10.1007/s00259-019-04527-w

ORIGINAL ARTICLE

Characterization of the serotonin 2A receptor selective PET tracer (R)-[^{18}F]MH.MZ in the human brain

Vasko Kramer[1,2] · Agnete Dyssegaard[3] · Jonathan Flores[1] · Cristian Soza-Ried[1] · Frank Rösch[4] · Gitte Moos Knudsen[3] · Horacio Amaral[1,2] · Matthias M. Herth[5,6]

Received: 30 April 2019 / Accepted: 5 September 2019 / Published online: 12 October 2019

Abstract

Purpose The serotonin receptor subtype 2A antagonist (5-HT$_{2A}$R) (R)-[^{18}F]MH.MZ has in preclinical studies been identified as a promising PET imaging agent for quantification of cerebral 5-HT$_{2A}$Rs. It displays a very similar selectivity profile as [^{11}C]MDL 100907, one of the most selective compounds identified thus far for the 5-HT$_{2A}$R. As [^{11}C]MDL 100907, (R)-[^{18}F]MH.MZ also displays slow brain kinetics in various animal models; however, the half-life of fluorine-18 allows for long scan times and consequently, a more precise determination of 5-HT$_{2A}$R binding could still be feasible. In this study, we aimed to evaluate the potential of (R)-[^{18}F]MH.MZ PET to image and quantify the 5-HT$_{2A}$R in the human brain in vivo.

Methods Nine healthy volunteers underwent (R)-[^{18}F]MH.MZ PET at baseline and four out of these also received a second PET scan, after ketanserin pretreatment. Regional time–activity curves of 17 brain regions were analyzed before and after pretreatment. We also investigated radiometabolism, time-dependent stability of outcomes measures, specificity of (R)-[^{18}F]MH.MZ 5-HT$_{2A}$R binding, and performance of different kinetic modeling approaches.

Results Highest uptake was determined in 5-HT$_{2A}$R rich regions with a BP$_{ND}$ of approximately 1.5 in cortex regions. No radiometabolism was observed. 1TCM and 2TCM resulted in similar outcome measure, whereas reference tissue models resulted in a small, but predictable bias. (R)-[^{18}F]MH.MZ binding conformed to the known distribution of 5-HT$_{2A}$R and could be blocked by pretreatment with ketanserin. Moreover, outcomes measures were stable after 100–110 min.

Conclusion (R)-[^{18}F]MH.MZ is a suitable PET tracer to image and quantify the 5-HT$_{2A}$R system in humans. In comparison with [^{11}C]MDL 100907, faster and more precise outcome measure could be obtained using (R)-[^{18}F]MH.MZ. We believe that (R)-[^{18}F]MH.MZ has the potential to become the antagonist radiotracer of choice to investigate the human 5-HT$_{2A}$R system.

Keywords [^{18}F]MH.MZ · MDL 100907 · 5-HT$_{2A}$ receptor · Positron emission tomography (PET) · Kinetic modeling

This article is part of the Topical Collection on Neurology

Electronic supplementary material The online version of this article (https://doi.org/10.1007/s00259-019-04527-w) contains supplementary material, which is available to authorized users.

✉ Vasko Kramer
vkramer@positronpharma.cl

✉ Matthias M. Herth
matthias.herth@sund.ku.dk

[1] Center for Nuclear Medicine & PET/CT Positronmed, Providencia, 7501068 Santiago, Chile

[2] Positronpharma SA, Providencia, 7500921 Santiago, Chile

[3] Center for Integrated Molecular Brain Imaging, Rigshospitalet and University of Copenhagen, Blegdamsvej 9, 2100 Copenhagen, Denmark

[4] Institute of Nuclear Chemistry, Johannes Gutenberg-University, Fritz-Strassmann-Weg 2, 55128 Mainz, Germany

[5] Department of Drug Design and Pharmacology, University of Copenhagen, Jagtvej 160, 2100 Copenhagen, Denmark

[6] Department of Clinical Physiology, Nuclear Medicine & PET, Rigshospitalet, Blegdamsvej 9, 2100 Copenhagen, Denmark

Introduction

Serotonin (5-hydroxytryptamine, 5-HT) 2A receptors (5-HT_{2A}R) have been implicated in the pathophysiology of human diseases such as depression, Alzheimer's disease, or schizophrenia [1–3]. 5-HT_{2A}Rs mediate the hallucinogenic effect of recreational agonist drugs [4], and atypical antipsychotics are characterized by 5-HT_{2A}R antagonism [4]. Thus, the 5-HT_{2A}R system is of significant clinical interest.

Positron emission tomography (PET) is a powerful, non-invasive, in vivo molecular imaging technique capable of localizing and quantifying molecular drug targets such as receptors or enzymes. It is a valuable tool to study mechanistic causes of diseases, carry out diagnosis, and monitor the success of treatment approaches [5–8]. PET can also be used to quantify receptor occupancies of therapeutic drug interventions [9, 10]. Compared with other molecular imaging modalities, the sensitivity and selectivity of PET with respect to detection and quantification of specific drug targets are unmatched [11].

Several 5-HT_{2A}R PET-tracers have been developed over the years [12, 13] and are currently applied in various clinical studies [14–16]. The vast majority of clinical studies have so far been performed with [^{18}F]altanserin and [^{11}C]MDL 100907 [14, 17–24]. However, both PET-tracers have limitations. [^{18}F]altanserin gives rise to blood–brain barrier (BBB) crossing radiometabolites, which complicate its analysis [25]. [^{11}C]MDL 100907 does not have this problem and is a more specific 5-HT_{2A}R ligand [26–29]. But scan durations of at least 90 min are necessary in humans to obtain stable PET outcome measures [26]. Carbon-11 has a half-life of 20.4 min and long scan durations with this nuclide result in relatively low count rates at 90 min. In this respect, a potential radiotracer combining the superior selectivity and in vivo stability of MDL 100907 with the better isotopic properties of fluorine-18 would possibly create a highly valuable PET tracer [26]. Moreover, the half-life of fluorine-18 (109.7 min) would permit transportation of the tracer to other PET centers that do not possess a cyclotron. Consequently, such a tracer would facilitate widespread application. We have recently reported the development of an ^{18}F-labeled analogue of MDL 100907, (R)-[^{18}F]MH.MZ [30–33]. Evaluation studies in rodents and pigs showed that this radioligand combines the selectivity of MDL 100907 with the superior isotopic properties of fluorine-18.

We here present the first characterization of (R)-[^{18}F]MH.MZ as a PET tracer in healthy adult human volunteers. Metabolism, regional brain uptake, derivation of outcome measures, and the optimum kinetic modeling strategy are reported.

Materials and methods

Human subjects

Nine male healthy controls (HC) (mean ± SD age 28.0 ± 9.3 years; median = 23 years; range 20–47 years, all male) were included in total and participated in a dynamic baseline brain PET scan. For 5/9 HCs, arterial blood samples were obtained and the other 4/9 HCs (mean age 30 ± 8 years, 4 males) participated in a second PET study after ketanserin pretreatment. Study participants were recruited through newspaper advertisements. None of the subjects were active smokers, took psychoactive medication, nor did they have prior or current substance or alcohol abuse as evaluated by the interview. All studies were approved by the regional ethic committee (Comité Ético Cientifico, Servicio de Salud Metropolitano Oriente, permits 20150407 and 20170307) and all subjects provided written informed consent after receiving an explanation of the relevant study.

Radiochemistry

All reagents and solvents were purchased from Merck Millipore or Sigma Aldrich in pharmaceutical grade and precursors 1,2-ethane-di-tosylate; MDL-105725 and reference standard (R)-MH.MZ were purchased in chemical grade from Advanced Biochemical Compounds (ABX). Experimental conditions for the radiosynthesis of (R)-[^{18}F]MH.MZ were previously reported [34] and adapted for GMP-compliant production using the IBA Synthera™ platform. Briefly, (R)-[^{18}F]MH.MZ was produced via two-step labeling (production of [^{18}F]-2-fluoroethyl tosylate and fluoro-alkylation of MDL-105725 in 8 ± 2% RCY (n.d.c.) (SI Scheme 1), > 98% radiochemical purity and specific activities of 160 ± 110 GBq/μmol.

Magnetic resonance imaging acquisition

All subjects were scanned in a 1.5T magnetic resonance imaging (MRI) scanner from Gyroscan Intera, Phillips Medical System, Best, the Netherlands. 3D T1-weighted MR images (isotropic 1 × 1 × 1 mm resolution) were acquired using the following parameters: T1 protocol; repetition time = 7.3 ms; echo delay time 3.3 ms. inversion time = 815 ms, and flip angle = 8°. Images were used for co-registration and normalization of corresponding PET images.

Positron emission tomography scanning

PET protocol

All devices that were used to quantify radioactivity amounts were cross-calibrated with an internal standard. The mean ±

SD of the administered mass of (R)-[^{18}F/^{19}F]MH.MZ was 1.63 ± 1.52 μg (range, 0.34–5.17 μg) and the mean administered activity was 196.0 ± 16.0 MBq (range, 172.5–223.4 MBq). There were no adverse or clinically detectable pharmacologic effects in any of the nine HCs and no significant changes in vital signs were observed. For all nine HCs, a low-dose CT scan was performed for attenuation correction and a PET scan was acquired for 180 min in LIST mode (Biograph mCT Flow, Siemens Healthineers, Erlangen, Germany), started simultaneously with the intravenous bolus injection of (R)-[^{18}F]MH.MZ. The injection took approximately 6–10 s. Head movement was minimized with a polyurethane head fixation system during the scan duration.

For 5/9 HCs, arterial blood samples were obtained from a catheter placed in the radial artery of the arm opposite to the injection site. This catheter was used for input function measurement and metabolite analysis. One scan of the aforementioned had to be excluded due to early abort (at t = 110 min post-injection (p.i.)). Another scan was excluded from further data analysis since no arterial samples could be obtained after 30 min since blot clotting occurred within the blood line.

Input function measurement

Radioactivity in whole blood (WB) was continuously measured for up to 120 min p.i. using an automated blood sampling system (Twilite 2, Swisstrace, Menzingen, Switzerland) as shown in supplemental information (SI). The flowrate was changed stepwise from 5 mL/min (0–6 min p.i.), to 2.5 mL/min (6–11 min p.i.) to 0.33 mL/min (11–120 min p.i.). Measuring intervals changed from initially 1 s steps (0–2 min p.i.) to 20 s-steps (2–120 min p.i.). In addition, arterial blood samples (9 mL) were drawn manually at 5, 10, 20, 30, 40, 50, 60, 90, 120, 150, and 180 min p.i. The samples at 150 and 180 min were additionally used to complete the dataset for the WB radioactivity. Plasma was obtained by centrifugation (4000 rpm, 5 min at room temperature) of 8 mL arterial WB samples. Radioactivity in 0.75 mL WB and 0.75 mL plasma was measured using a well counter (CRC®-55tW Dose Calibrator/well counter, Capintec, Florham Park, USA) to calculate plasma/WB ratios. All radioactive samples were decay corrected to the time of radioligand injection.

Radiometabolite measurement

Method 1 (Plasma water injection into a HPLC system) The parent fraction of (R)-[^{18}F]MH.MZ in plasma was determined as described previously [35]. Briefly, to 1.5 mL of the obtained plasma fraction, 3.0 mL acetonitrile was added and the resulting suspension centrifuged (4000 rpm, 5 min) to remove soluble proteins. Two milliliters of the plasma water sample were injected directly into an analytical HPLC system from Agilent (1260 Isoc. Pump G1310B, Agilent 1260 UV detector Infinity VWD VL G1314B, Gabi Star radioactivity detector, Gina Star Software, both Raytest) equipped with a 2 mL sample loop and a Phenomenex Luna C18(2), 5 u, 150 × 4,6 mm column. The area under the peaks corresponding to radiometabolites and parent compound was quantified and expressed as a percentage of the sum of all detected areas.

Method 2 (Direct injection of plasma into a HPLC system) The parent fraction of (R)-[^{18}F]MH.MZ in plasma was determined by direct injection of plasma into a HPLC system, as previously described [36]. In order to adapt the procedure to our local system, we used an analytical HPLC system (described above) equipped with a 2 mL sample loop and an analytical column (Shimadzu Shim-pack MAYI-ODS(G) 30 × 4,6 mm). The plasma fraction was passed through a syringe filter (Whatman GD/X 13 mm, PVDF, 0.45 mm) and 2 mL filtered plasma was injected at a flow of 5 mL/min of solvent A (0.25 M ammonium acetate buffer pH = 4.5). After 5 min (extraction phase) the flow was stopped, a second column (Phenomenex Luna C18(2), 5 μ, 150 × 4,6 mm) inserted after the Shim-pack column. After 8 min the lipophilic compounds were eluted at 2 mL/min with solvent B (45% acetonitrile, 55% solvent A). Radiometabolite/parent compound analysis was carried out as described in method 1.

Image reconstruction and post-processing

PET images were corrected for scatter, attenuation, and TOF and reconstructed by an iterative ordered-subsets expectation maximization algorithm (2 iterations and 21 subsets) followed by post-construction smoothing Gaussian filer (4 mm full-width at one-half maximum). The whole study was reframed into 46 dynamic frames (6 × 10 s, 6 × 20 s, 6 × 60 s, 5 × 120 s, 14 × 300 s, and 9 × 600 s frames). Images consisted of 110 planes of 256 × 256 voxels of 1.59 × 1.59 × 1.5 mm^3. PET Images were reviewed and corrected for motion by matching individual frames to an averaged image from 0 to 3 min post-injection using an automated algorithm (PFuse, PMod Technologies LLC, Zürich, Switzerland). Volumes of interest were generated from three-dimensional maximum probability atlas [37] after co-registration and normalization using (PNeuro, PMod Technologies LLC, Zürich, Switzerland). For quantification, time–activity curves were generated for relevant brain VOIs (13 high-density binding regions such as temporal cortex, frontal cortex, or parietal cortex, hippocampus as a medium-density binding region, and thalamus, striatum, and cerebellum as low-density binding regions). For the respective time–activity curves, standardized uptake values (SUVs) were obtained by normalizing radioactive concentrations in VOIs (extracted as kBq/mL) to the injected dose per body weight (in kBq/g) yielding the unit g/mL.

Quantification of (R)-[^{18}F]MH.MZ binding

Kinetic modeling was performed (PKin, PMod Technologies Ltd., Zürich, Switzerland) using radioactive concentrations in WB, plasma, and parent compound fraction as an input to fit tissue time–activity curves. All blood measurements were referenced to the time of injection. The arterial input function was derived as described above. (R)-[^{18}F]MH.MZ distribution volumes (V_T) were derived from the one- and two-tissue compartment models (1TCM and 2TCM) fitting three (K_1, k_2, V_B) or five parameters (K_1, k_2, k_3, k_4, V_B), respectively. In all subjects, the PET camera was synchronized with the blood sampler for acquisition of the arterial input function previous to tracer injection. (R)-[^{18}F]MH.MZ V_Ts were also calculated from linearization with Logan plot graphical analyses. The non-displaceable binding potentials BP_{ND} for the 2TCM were derived from V_T in high and low target areas as follows: $(V_T^{target} - V_T^{cerebellum})/V_T^{cerebellum}$. BP_{ND}s were calculated with the Logan plot non-invasive GA (NIGA), multilinear reference tissue model (MRTM0) and the simplified reference tissue model (SRTM). The cerebellum was used as reference tissue for all BP_{ND} determinations. All applied kinetic models are described in detail in (38, 39). Goodness-of-fit was evaluated using the Akaike Information Criterion (AIC).

Stability of outcome measures

Experimental data were collected for 180 min. V_T as outcome measure (2TCM) was evaluated depending on the duration of the scan by truncating the tissue time–activity curves (TAC) in 10-min increments (from 180 to 60 min) to simulate shorter scans and comparing the results with the reference value obtained with the 180-min dataset. For each region and each scan duration the mean ± SD ($n = 3$) of the results expressed as a percentage of the reference value was calculated to provide an estimate of the bias that is induced using shorter scan times. V_T was considered stable relative to scan duration after time t if all results derived from time t to 180 min had a mean within 5% of the reference value.

5-HT$_{2A}$R specificity

The 5-HT$_{2A}$R specificity of (R)-[^{18}F]MH.MZ was investigated by comparison of the baseline PET with a second (R)-[^{18}F]MH.MZ PET scan after ketanserin pretreatment (scan duration 180 min) about 2 weeks apart. The cerebellum was used as a reference region devoid of 5-HT$_{2A}$Rs [11, 25, 27, 28, 40]. Four HCs received an oral blocking dose of 10 mg ($n = 1$) or 20 mg ($n = 3$) ketanserin (ketanserin, Janssen-Cilag, the Netherlands) 45 ± 1 min before a second (R)-[^{18}F]MH.MZ PET scan with the same PET protocol was performed. No adverse reactions that could be related to ketanserin administration were observed. One-fourth of the subjects who received 10 mg ketanserin was not able to complete the whole imaging protocol. Data from this scan was excluded from further analysis.

Statistical analysis

To analyze the specificity of (R)-[^{18}F]MH.MZ, we used unequal variance two-tailed unpaired Student's t test to compare baseline PET BP_{ND}s with BP_{ND} values from a second (R)-[^{18}F]MH.MZ PET scan after ketanserin pretreatment. Both events were considered independent and all cortex tissues were included in the analysis. For comparison between models regarding V_t and BP_{ND}, we use the Kruskal–Wallis and the Dunn multiple comparison as a post hoc non-parametric test. To analyze differences between models regarding AIC criteria, we used two-tailed unpaired Student's t test. To assess the equality of variances between groups, Levene's test was used. In all the comparisons the results were considered significant when P values were less than 0.05. All comparison analyses were performed using STATA, version 14.

Results

Plasma analysis and metabolism

The estimated parent plasma input function (mean ± SD, $n = 3$) is shown in Fig. 1a. After i.v. bolus injection of (R)-[^{18}F]MH.MZ, WB and plasma total activity peaked rapidly after approximately 1 min at 25 ± 4 and 20 ± 3 kBq/cc, respectively, and decreased quickly to a minimum at 5.2 min of 2.3 ± 0.6 and 1.9 ± 0.5 kBq/cc, respectively (Fig. 1a). Afterwards, (R)-[^{18}F]MH.MZ activity in WB and plasma decreased very slowly and remained almost stable until the end of the scan. Plasma-to-WB activity ratio was stable within 0–180 min p.i. at a ratio of 0.814 ± 0.046 (mean ± SD, $n = 3$, SI Table 3). We detected only parent compound of (R)-[^{18}F]MH.MZ throughout the entire duration of the PET study (see Fig. 1c). This result was verified using two different analysis methods (see methods and SI) and the unmetabolized parent fraction in plasma is constant at 100% during the sampling duration (see Fig. 1b). Consequently, the plasma input function could be used without further metabolite correction for modeling purposes.

(R)-[^{18}F]MH.MZ brain distribution

(R)-[^{18}F]MH.MZ readily entered the human brain and accumulated over time in brain regions with the expected human

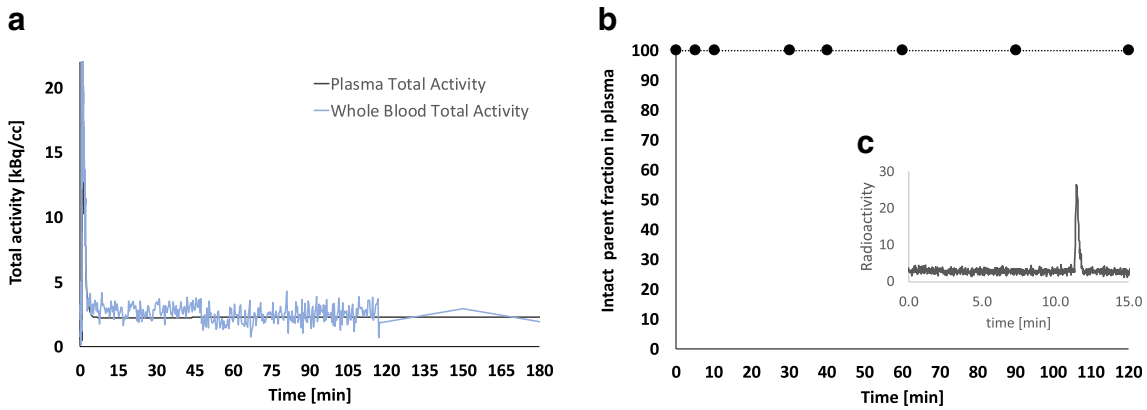

Fig. 1 **a** WB total activity, mean of 3 measurements derived from 3 subjects. **b** Fraction of unmetabolized (R)-[^{18}F]MH.MZ in arterial plasma ($n = 3$). **c** Representative analytical RadioHPLC chromatogram, only parent compound was detected

cerebral 5-HT$_{2A}$R distribution pattern (Fig. 2a). Highest (R)-[^{18}F]MH.MZ binding was found in cortical regions. Intermediate binding was found in the hippocampus, whereas in other subcortical regions (for example, the thalamus or striatum) and in the cerebellum, gray matter binding was comparably low.

In neocortical regions and the insula, (R)-[^{18}F]MH.MZ peak uptake was observed after 78 ± 21 min (mean ± SD, $n = 8$). Within the 180 min scanning time frame, tracer washout (as defined as percentage activity decrease from peak to the end of the scan in a specific region) was determined to be in the range of 1–18%. Peak uptake in the striatum, thalamus, and cerebellum was reached earlier (9–22 min). Tracer washout was relatively higher (37–54%). Peak uptake in the hippocampus was observed after 25–42 min and tracer washout has been determined to between 12 and 32% (Fig. 2b).

Kinetic modeling of (R)-[^{18}F]MH.MZ binding

Time–activity curves were analyzed for goodness-of-fit by visual inspection and model performance by comparison of AIC values. Kinetic modeling using 2TCM resulted in slightly higher distribution volumes (V_Ts) for (R)-[^{18}F]MH.MZ binding when compared with 1TCM and Logan. Nevertheless, all models gave similar results and the difference was not statistically significant. The results for AIC criteria driven from 1TCM and 2TCM were similar and no significant difference could be observed (Table 1 and Fig. 3). All non-invasive reference tissue models (SRTM, MRTM0, and NIGA) generated significantly higher non-displaceable binding potentials (BP_{ND}s) than those derived from invasive 2TCM ($P < 0.05$) (see Fig. 3c–e). Within the non-invasive models, MRTM0 resulted in slightly higher BP_{ND} values than SRTM followed

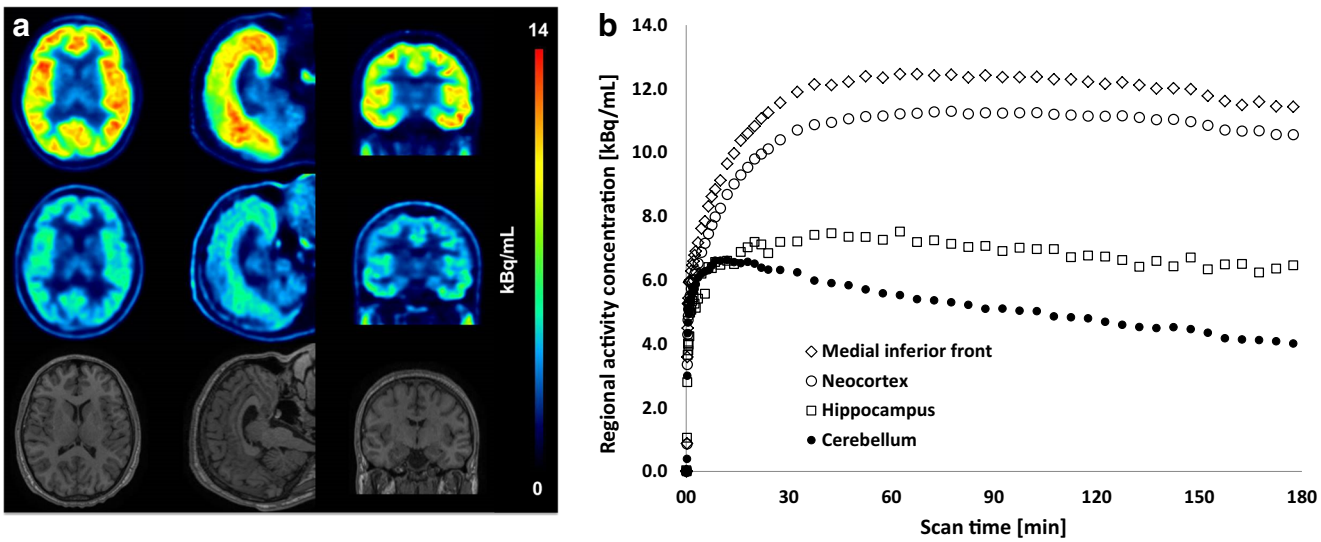

Fig. 2 **a** Representative (R)-[^{18}F]MH.MZ PET brain images from a HC (subject 2). Transversal, sagittal and coronal images (from left to right) are displayed from averaged frames between 150 and 180 min post-injection. Images are scaled to 0-14 kBq/cc (equivalent to SUV-ratio 0-4). Upper row: baseline PET scan; middle row: PET scan after oral administration of 20 mg ketanserin 45 min prior to injection of (R)-[^{18}F]MH.MZ; lower row: T1-weighted MRI images. **b** Representative (R)-[^{18}F]MH.MZ tissue time–activity curves from a HC (subject 2)

Table 1 Total (R)-[^{18}F]MH.MZ V_T estimated using 2TCM, 1TCM, Logan graphical analysis with arterial input function, and BP_{ND} estimated using 2TCM, NIGA, MRTM0, and SRTM, mean ± SD, $n = 3$

	Total distribution volumes (VT)			Non-displaceable binding potential (BPnd)			
	2TCM	1TCM	Logan	2TMC	NIGA	MRTM0	SRTM
	V_T (mL/cm^3)	V_T (mL/cm^3)	V_T (mL/cm^3)	BP_{ND} (unitless)	BP_{ND} (unitless)	BP_{ND} (unitless)	BP_{ND} (unitless)
Medial_inferior_temporal_gyrus	5.09 ± 1.72	4.99 ± 1.81	4.76 ± 1.58	0.94 ± 0.13	1.37 ± 0.20	1.58 ± 0.23	1.46 ± 0.19
Orbito_frontal_cortex	4.97 ± 1.81	4.98 ± 1.96	4.72 ± 1.70	0.88 ± 0.13	1.29 ± 0.23	1.41 ± 0.26	1.36 ± 0.23
Temporal_cortex	4.58 ± 1.60	4.52 ± 1.64	4.32 ± 1.45	0.74 ± 0.10	1.12 ± 0.16	1.29 ± 0.18	1.21 ± 0.15
Anterior_cingulate	4.64 ± 1.31	4.53 ± 1.35	4.33 ± 1.17	0.79 ± 0.20	1.24 ± 0.31	1.42 ± 0.45	1.34 ± 0.37
Superior_temporal_gyrus	4.89 ± 1.92	4.82 ± 1.95	4.61 ± 1.73	0.84 ± 0.16	1.22 ± 0.19	1.39 ± 0.21	1.32 ± 0.19
Insula	4.30 ± 1.71	4.25 ± 1.66	4.07 ± 1.48	0.62 ± 0.11	1.03 ± 0.21	1.18 ± 0.25	1.13 ± 0.22
Medial_inferior_frontal_gyrus	5.18 ± 1.62	5.36 ± 2.02	5.09 ± 1.78	0.99 ± 0.20	1.50 ± 0.30	1.68 ± 0.44	1.60 ± 0.36
Frontal_cortex	5.14 ± 1.88	5.10 ± 1.90	4.84 ± 1.66	0.95 ± 0.17	1.36 ± 0.27	1.52 ± 0.35	1.45 ± 0.30
Superior_frontal_gyrus	5.14 ± 1.86	5.09 ± 1.91	4.83 ± 1.68	0.95 ± 0.20	1.37 ± 0.32	1.56 ± 0.47	1.47 ± 0.40
Neocortex	4.92 ± 1.76	4.87 ± 1.77	4.63 ± 1.55	0.87 ± 0.14	1.26 ± 0.21	1.41 ± 0.26	1.34 ± 0.22
Posterior_cingulate	5.37 ± 1.70	5.33 ± 1.73	5.07 ± 1.52	1.06 ± 0.23	1.55 ± 0.34	1.71 ± 0.44	1.65 ± 0.39
Parietal_cortex	4.86 ± 1.72	4.85 ± 1.73	4.61 ± 1.51	0.85 ± 0.18	1.27 ± 0.22	1.41 ± 0.28	1.34 ± 0.24
Occipital_cortex	5.03 ± 1.82	4.96 ± 1.76	4.73 ± 1.55	0.90 ± 0.09	1.26 ± 0.16	1.40 ± 0.18	1.33 ± 0.16
Hippocampus	2.98 ± 1.00	2.96 ± 0.99	2.77 ± 0.90	0.13 ± 0.04	0.28 ± 0.09	0.30 ± 0.10	0.30 ± 0.10
Thalamus	2.79 ± 0.84	2.76 ± 0.84	2.44 ± 0.75	0.07 ± 0.07	0.08 ± 0.05	0.08 ± 0.08	0.09 ± 0.05
Striatum	2.69 ± 0.99	2.65 ± 0.96	2.38 ± 0.93	0.01 ± 0.02	0.02 ± 0.03	0.02 ± 0.03	0.16 ± 0.40
Cerebellum	2.66 ± 0.98	2.63 ± 0.95	2.38 ± 0.91				

Mean ± standard deviation of 3 subjects are shown for each model. *2TCM*, two-tissue compartment model; *1TCM*, one-tissue compartment model; *BP_{ND}*,: non-displaceable binding potential; *MRT0*, multi-linear reference tissue model; *NIGA*, non-invasive graphical analyses; *SRTM*, simplified reference tissue model. All BP_{ND}s are measured uses cerebellum as reference region.

by NIGA, although the difference was not significant. Nevertheless, SRTM resulted in a better fit, indicated by lower AIC criteria values in the medial inferior temporal lobe, orbital frontal cortex, temporal cortex, superior temporal gyrus, neocortex, parietal cortex, occipital cortex, hippocampus, and thalamus ($P < 0.05$).

Stability of outcome measures

To investigate which minimal scanning time is needed to derive stable outcome measures for each region, tissue time–activity curves were truncated in 10-min increments (from 180 to 60 min). Afterwards, each time–activity curve was used to derive V_T values applying 2TCM. These values were compared. Cortical V_T values calculated for high binding region were stable within shorter scan durations up to 60 to 70 min, whereas V_T values for low binding regions like the thalamus, striatum, and cerebellum were overestimated at shorter scan durations. Higher deviations as 5% were found with decreased scan times of 140, 110, and 100 min, respectively. The V_T values in the hippocampus were stable after scan times of 80 min. Scan time reduction from 180 to 60 min did not lead to a bias of more than 10% deviation of V_T values in any of the cortical regions. Figure 4 summarizes the obtained results.

Specificity of (R)-[^{18}F]MH.MZ binding

The 5-HT_{2A}R specificity of (R)-[^{18}F]MH.MZ binding was determined by comparing BP_{ND} values derived from SRTM for individual brain regions from baseline PET scans with BP_{ND} values after selective ketanserin pretreatment. BP_{ND} after pretreatment was significantly reduced in 5-HT_{2A}R high-density, cortical regions and the medium-density region hippocampus ($P < 0.001$), but unaltered in low binding regions such as the striatum or thalamus (Fig. 5). It should be mentioned that non-specific binding within the reference regions, such as the cerebellum, increased after blockade of 5-HT_{2A}Rs by ketanserin. This increased uptake in cerebellum can be explained by displacement or blockage of peripheral 5-HT_{2A}R binding sites.

Discussion

We present here the first evaluation of (R)-[^{18}F]MH.MZ as a PET imaging agent of the 5-HT_{2A}R in the human brain. Regarding the inclusion criteria, it has been shown that the mean rate of serotonin synthesis in males is about 52% higher than in females, which may be a factor relevant to the lower incidence of major unipolar depression in males [41]. Those results are in line

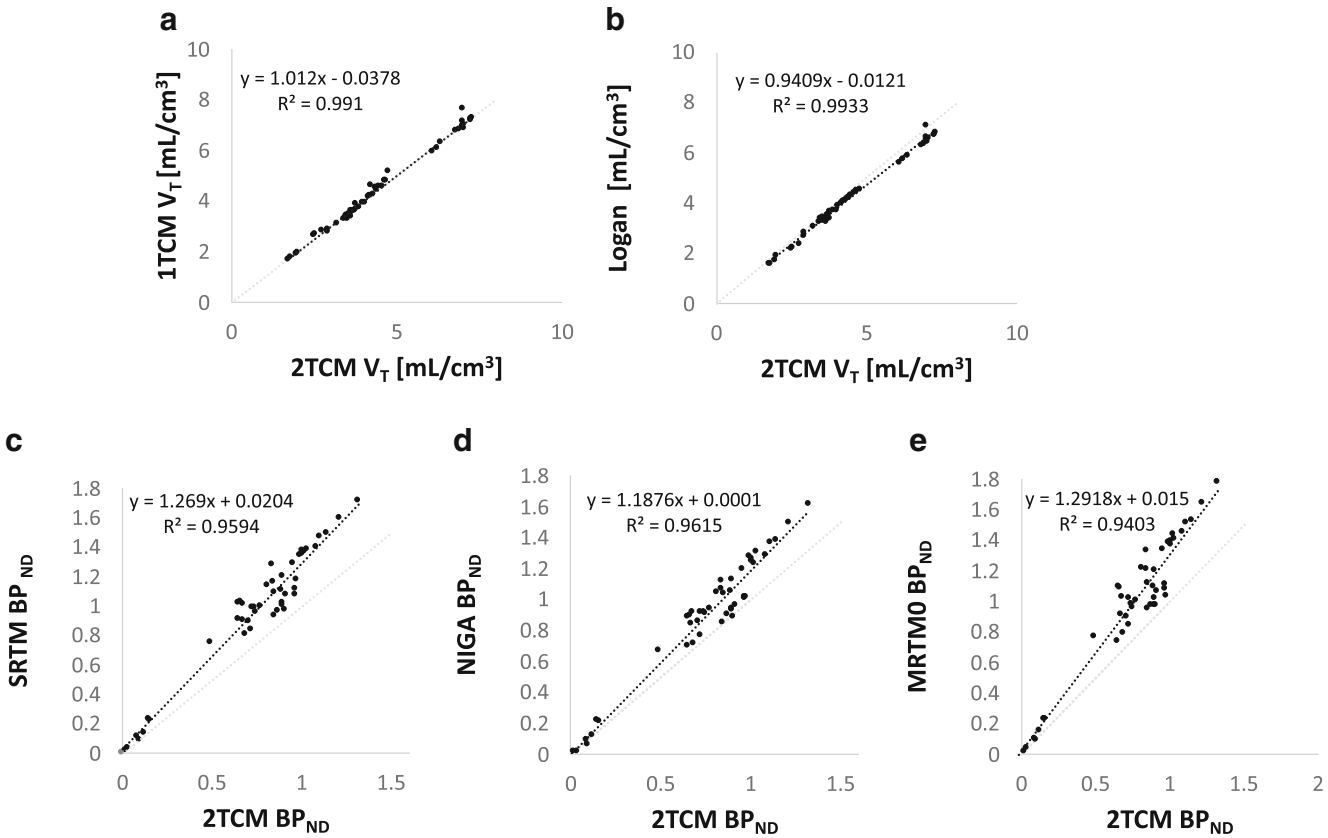

Fig. 3 Linear regression analyses displays the correlation between outcome measures V_T **a**, **b** and BP_{ND} **c**, **d**, **e** determined by linear **b**, **d** and non-linear models **a**, **c**, **e**. Outcome measures were obtained using 2TCM fitting five parameters (K_1, k_2, k_3, k_4, V_b). In V_T estimations, 17 regions (see Table 1) were analyzed from 3 subjects. The cerebellum was used as a reference region for all BP_{ND} estimations. BP_{ND} for the 2TCM was calculated as $(V_T^{target}-V_T^{cerebellum})/V_T^{cerebellum}$. Black-dotted lines show linear regression. The regression equation for each correlation is displayed in each plot. Gray-dotted lines represent line of identity

with previous PET studies which reported higher V_ts in female subjects when compared with male subjects [42]. We, therefore, decided to include only male subjects in our study.

Our data show that (R)-[^{18}F]MH.MZ can be used to image and quantify the 5-HT_{2A}R system in high, but also in low receptor density areas. The affinity and selectivity of

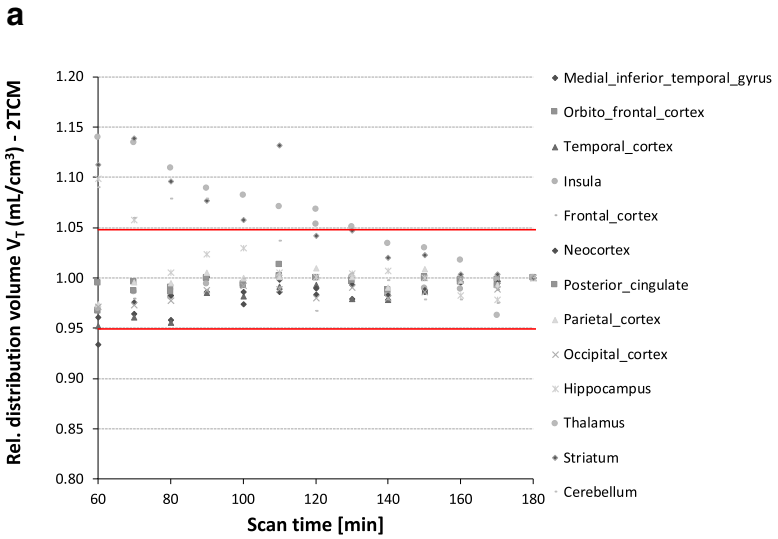

b

Time to stable outcome measures [min]	2TCM V_T (mL/cm^3)
Medial_inferior_temporal_gyrus	70
Orbito_frontal_cortex	60
Temporal_cortex	60
Anterior_cingulate	70
Superior_temporal_gyrus	60
Insula	130
Medial_inferior_frontal_gyrus	60
Frontal_cortex	60
Superior_frontal_gyrus	60
Neocortex	60
Posterior_cingulate	60
Parietal_cortex	60
Occipital_cortex	60
Hippocampus	80
Thalamus	140
Striatum	110
Cerebellum	100

Fig. 4 Minimal scanning time (minutes) needed to derive stable estimates of V_Ts determined by the 2TC model. **a** Correlation between the relative distribution volume and scan duration. **b** Minimal time needed to derive at stable outcome measure for respective brain regions with a permitted deviation of 5%

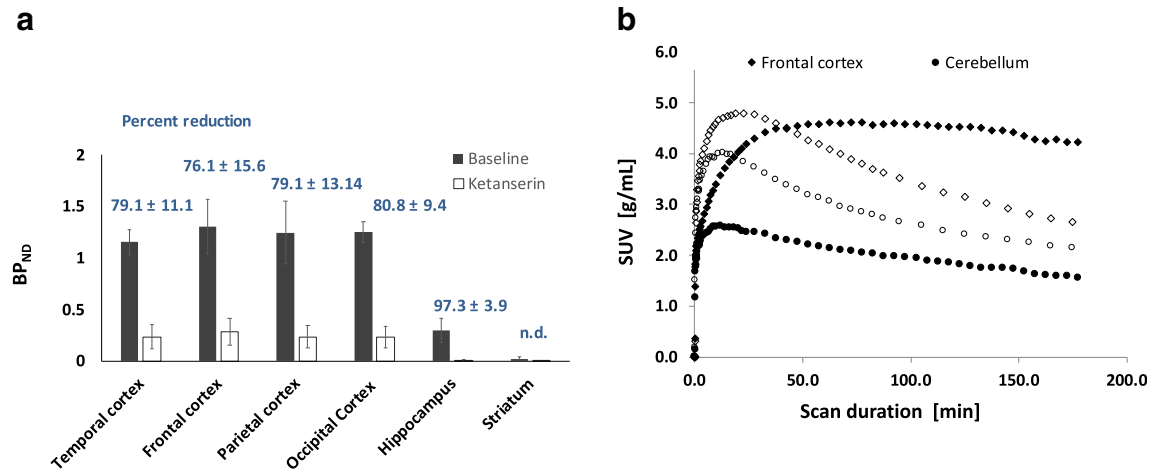

Fig. 5 **a** (R)-[^{18}F]MH.MZ BP$_{ND}$s derived from SRTM at baseline ($n = 3$) and after oral ketanserin pretreatment (20 mg, $n = 3$). BP$_{ND}$s are significantly lower in cortical regions and the hippocampus ($P < 0.05$). **b** Representative (R)-[^{18}F]MH.MZ tissue time–activity curves from a HC (subject 2) at baseline and intervention with 20 mg ketanserin pretreatment 45 min prior to scanning

(R)-[^{18}F]MH.MZ is comparable with that of MDL 100907, one of the most 5-HT$_{2A}$R selective ligands identified so far [12]. Brain activity uptake of (R)-[^{18}F]MH.MZ was highest in cortical regions and low in the striatum, hippocampus, thalamus, and cerebellum. This distribution is in line with the reported human 5-HT$_{2A}$R brain distribution [26–28, 40].

[^{18}F]altanserin, the most widely used PET tracer for 5-HT$_{2A}$Rs, gives rise to lipophilic metabolites which are able to cross the BBB and complicate quantitative analysis. To solve this problem, a bolus infusion approach has been developed and validated and can be used for quantification [25]. Nevertheless, the need for infusion of the tracer over time is impractical and inconvenient as compared with standard bolus injection. For quantitative analysis of [^{11}C]MDL 100907 binding to 5-HT$_{2A}$Rs, invasive 2TCM is the method of choice and stable V_Ts can be obtained after 90 min p.i. in most brain regions [26]. Nevertheless, due to the short half-life of ^{11}C (20.4 min), count rates in the late stages of the scan are very low and represent a disadvantage [26, 27].

In contrast to [^{11}C]MDL 100907 and [^{18}F]altanserin, (R)-[^{18}F]MH.MZ displays no detectable metabolism in human plasma over a timeframe of 180 min. This was unexpected since (R)-[^{18}F]MH.MZ is rapidly metabolized in rodents and pigs [30, 31], at a rate similar to that of [^{11}C]MDL 100907 which has a plasma half-live of approximately 5 min. Tracers with no metabolites can facilitate kinetic modeling approaches. Firstly, no compensatory methods are needed to take into account blood brain-barrier penetrant radiometabolites [25–27]. Secondly, invasive blood sampling to determine the arterial input function can be done without labor intensive plasma metabolite analyses that also is prone to induce noise [26–28]. Thirdly, image-derived (from heart cavities or other reference tissues) input functions can be used to assess the arterial input [43]. The flip side of the metabolically stable [^{18}F]MH.MZ is that it results in slow TACs. This is because (R)-[^{18}F]MH.MZ continuously accumulates from blood into the brain over the whole scan time (Fig. 2b).

We found that 1TCM as well as 2TCM based on arterial input measurements are optimal for quantification of (R)-[^{18}F]MH.MZ. Both models resulted in very similar outcome measures (Fig. 3), provided good fits for all TACs and showed the lowest AIC values. Logan graphical analysis resulted in similar outcome measures; however, values were slightly underestimated. Quantitative analysis using reference tissue models such as SRTM, NIGA, and MRTM showed excellent correlation ($R^2 > 0.959$, 0.961, and 0.940, respectively), but induced a positive bias (27%, 19%, and 29%, respectively) as compared with BP$_{ND}$ derived from the 2TCM. In contrast, the use of reference tissue models for quantification of [^{11}C]MDL 100907 resulted in good correlation but significant underestimation of 5-HT$_{2A}$R availability as compared with 2TCM [27]. The authors therefore encourage the use of 2TCM for precise quantification, but conclude that reference models such as SRTM or NIGA provide good estimates for between-group or between-condition comparison [26, 27]. Similarly, the induced positive bias for (R)-[^{18}F]MH.MZ is constant and predictable across all brain regions, and reference models can therefore be applied in studies comparing HCs and patients. This would be beneficial in clinical studies where arterial cannulation is often impractical. Furthermore, reference tissue models typically result in higher test–retest reproducibility and lower variability [11].

We also evaluated the optimal scan duration and the necessity for 180 min scans by shortening time–activity curves in 10 min increments and repeated kinetic modeling with 2TCM. In general, V_T outcome values were very stable even at shorter scan durations. V_Ts in cortical regions were stable after approximately 60 min, whereas V_Ts in lower binding regions such as the striatum or cerebellum were stable after 100–110 min, accepting a 5% deviation. Increasing the deviation to

10%, stable V_Ts were observed in all regions after 80–90 min. Given the half-life of fluorine-18 (110 min), necessary scan times are easily conductible using (R)-[^{18}F]MH.MZ. This is an advantage of this tracer compared with its carbon-11 analogue, [^{11}C]MDL 100907, where scan times of 90 min are necessary to derive at stable outcomes measure with a permitted deviation < 15% [26]. Lower deviation below 5% would not result in stable outcome measure before approximately 110 min. At this time, only low count rates can be observed with carbon-11 and results may as such be prone to error.

In contrast, when looking at the impact of scan duration on BP_{ND} values derived from reference models, we found that no stable BP_{ND} values could be obtained within the 180 min scan duration (see Figs. 7, 8, and 9 in SI). We attribute this to the metabolically stable derivative (R)-[^{18}F]MH.MZ, resulting in slower kinetics and slower washout from high density and reference regions as compared to [^{11}C]MDL 100907. This causes increasing BP_{ND} values over time and a variable bias depending on the imaging protocol, which may represent a limitation for the applicability of reference models for precise quantification. Nevertheless, as other studies emphasized, reference models may still provide good estimates for between-group comparisons [26, 27].

Selective binding of (R)-[^{18}F]MH.MZ was tested by pretreatment with 20 mg ketanserin and resulted in a profound block of all 5-HT_{2A}R high- and medium-density brain regions (80–97%). A lower blocking effect was observed in high binding regions and is most likely due to the fact that the amount of ketanserin was not sufficient enough to saturate all binding sites in these regions. We decided to use 20 mg of ketanserin because for the two 5-HT_{2A}R radiotracers [^{11}C]Cimbi-36 and [^{18}F]altanserin, binding is successfully blocked with a similar dose [11, 25, 44]. In the case of [^{11}C]MDL 100907, similar blocking effects have been observed using a slightly higher ketanserin dose [45]. We believe that a higher ketanserin dose would lead to a complete block of all 5-HT_{2A}Rs also in high-density regions. Further studies are needed to verify this hypothesis. However, our results strongly indicate that (R)-[^{18}F]MH.MZ binds selectively to 5-HT_{2A}Rs in the human brain. An approximate signal-to-noise ratio of 2.1–2.6 was detected in cortical regions. This signal-to-background is similar to the ratios of [^{11}C]MDL 100907 [26].

Conclusion

(R)-[^{18}F]MH.MZ is a highly selective 5-HT_{2A}R PET ligand that is able to detect and quantify 5-HT_{2A}Rs in the human brain. High brain uptake, good contrast, and absence of radiolabeled metabolites are beneficial characteristics of (R)-[^{18}F]MH.MZ for clinical applications. Stable outcome measures were observed after 100–110 min. Scan duration of such timeframes are easily achievable with a fluorine-18 tracer. 1TCM or 2TCM kinetic model are suitable for (R)-[^{18}F]MH.MZ quantification. Both models result in similar outcomes. Reference models appear to slightly overestimate outcome measures. Future studies are warranted to investigate if this bias is predictable and can be accounted. The absence of radiolabeled metabolites omits metabolite analysis and has the potential to substitute arterial input functions with image-derived inputs, from heart cavities or other reference tissue. In summary, we believe that (R)-[^{18}F]MH.MZ has favorable properties to image the 5-HT_{2A}R system in humans and could be used in the future to study the 5-HT_{2A}R system in HCs and patients.

Acknowledgments The authors would like to thank Dr. Geoff Warnock from PMod Technologies, Switzerland, for his input regarding blood sampling and data evaluation as well as Dr. Evelyng Faure Lobos for acquiring the MRI scans at the Imaging Department of FALP (Instituto Oncológico Fundación Arturo López Pérez), Santiago de Chile, Chile. We also thank Carlos Elgueta and Dr. Mario Avila from Positronpharma for the assistance in tracer production and Irene Coudeu and Ana Hurtado for their help with technical issues.

Funding information This study was in part funded by the Savværksejer Jeppe Juhls og Hustru Ovita Juhls foundation.

Compliance with ethical standards

Conflict of interest The authors declare that they have no conflict of interest.

Ethical approval All procedures performed in studies involving human participants were in accordance with the ethical standards of the institutional and/or national research committee (Comité Ético Cientifico, Servicio de Salud Metropolitano Oriente, permits 20150407 and 20170307) and with the principles of the 1964 Declaration of Helsinki and its later amendments or comparable ethical standards. Informed consent was obtained from all individual participants included in the study.

References

1. Naughton M, Mulrooney JB, Leonard BE. A review of the role of serotonin receptors in psychiatric disorders. Hum Psychopharmacol Clin Exp. 2000;15(6):397–415.
2. Nichols DE, Nichols CD. Serotonin receptors. Chem Rev. 2008;108(5):1614–41.
3. Marazziti D. Understanding the role of serotonin in psychiatric diseases. F1000Res. 2017;6:180.
4. Gonzalez-Maeso J, Sealfon SC. Psychedelics and schizophrenia. Trends Neurosci. 2009;32(4):225–32.
5. Piel M, Vernaleken I, Rosch F. Positron emission tomography in CNS drug discovery and drug monitoring. J Med Chem. 2014;57(22):9232–58.
6. Schrevens L, Lorent N, Dooms C, Vansteenkiste J. The role of PET scan in diagnosis, staging, and management of non-small cell lung cancer. Oncologist. 2004;9(6):633–43.
7. Pennant M, Takwoingi Y, Pennant L, Davenport C, Fry-Smith A, Eisinga A, et al. A systematic review of positron emission tomography (PET) and positron emission tomography/computed tomography (PET/CT) for the diagnosis of breast cancer recurrence. Health Technol Assess. 2010;14(50):1–103.

8. Kristensen JL, Herth MM. Textbook of drug design and discovery: in vivo imaging in drug discovery. Fifth edition ed 2017.
9. Paterson LM, Tyacke RJ, Nutt DJ, Knudsen GM. Measuring endogenous 5-HT release by emission tomography: promises and pitfalls. J Cereb Blood Flow Metab. 2010;30(10):1682–706.
10. Skinbjerg M, Sibley DR, Javitch JA, Abi-Dargham A. Imaging the high-affinity state of the dopamine D_2 receptor in vivo: fact or fiction? Biochem Pharmacol. 2012;83(2):193–8.
11. Ettrup A, da Cunha-Bang S, McMahon B, Lehel S, Dyssegaard A, Skibsted AW, et al. Serotonin 2A receptor agonist binding in the human brain with [^{11}C]Cimbi-36. J Cereb Blood Flow Metab. 2014;34(7):1188–96.
12. Herth MM, Knudsen GM. Current radiosynthesis strategies for 5-HT_{2A} receptor PET tracers. J Label Compd Radiopharm. 2015;58(7):265–73.
13. Grunder G, Yokoi F, Offord SJ, Ravert HT, Dannals RF, Salzmann JK, et al. Time course of 5-HT_{2A} receptor occupancy in the human brain after a single oral dose of the putative antipsychotic drug MDL 100907 measured by positron emission tomography. Neuropsychopharmacology. 1997;17(3):175–85.
14. Paterson LM, Kornum BR, Nutt DJ, Pike VW, Knudsen GM. 5-HT radioligands for human brain imaging with PET and SPECT. Med Res Rev. 2013;33(1):54–111.
15. Madsen MK, Fisher PM, Burmester D, Dyssegaard A, Stenbaek DS, Kristiansen S, et al. Psychedelic effects of psilocybin correlate with serotonin 2A receptor occupancy and plasma psilocin levels. Neuropsychopharmacology. 2019.
16. Stenbaek DS, Kristiansen S, Burmester D, Madsen MK, Frokjaer VG, Knudsen GM, et al. Trait openness and serotonin 2A receptors in healthy volunteers: a positron emission tomography study. Hum Brain Mapp 2019.
17. Kehne JH, Baron BM, Carr AA, Chaney SF, Elands J, Feldman DJ, et al. Preclinical characterization of the potential of the putative atypical antipsychotic MDL 100907 as a potent 5-HT_{2A} antagonist with a favorable CNS safety profile. J Pharmacol Exp Ther. 1996;277(2):968–81.
18. Herth MM, Kramer V, Piel M, Palner M, Riss PJ, Knudsen GM, et al. Synthesis and in vitro affinities of various MDL 100907 derivatives as potential ^{18}F-radioligands for 5-HT_{2A} receptor imaging with PET. Bioorg Med Chem. 2009;17(8):2989–3002.
19. Leysen JE. Use of 5-ht receptor agonists and antagonists for the characterization of their respective receptor sites. In: Boulton A, Baker G, Juorio A, editors. Drugs as tools in neurotransmitter research. Neuromethods. 12: Humana Press; 1989. p. 299–350.
20. Bhagwagar Z, Hinz R, Taylor M, Fancy S, Cowen P, Grasby P. Increased 5-HT_{2A} receptor binding in euthymic, medication-free patients recovered from depression: a positron emission study with [^{11}C]MDL 100,907. Am J Psychiatry. 2006;163(9):1580–7.
21. Hirani E, Sharp T, Sprakes M, Grasby P, Hume S. Fenfluramine evokes 5-HT_{2A} receptor-mediated responses but does not displace [^{11}C]MDL 100907: small animal PET and gene expression studies. Synapse. 2003;50(3):251–60.
22. Ito H, Nyberg S, Halldin C, Lundkvist C, Farde L. PET imaging of central 5-HT_{2A} receptors with [^{11}C]MDL 100907. J Nucl Med. 1998;39(1):208–14.
23. Watabe H, Channing MA, Der MG, Adams HR, Jagoda E, Herscovitch P, et al. Kinetic analysis of the 5-HT_{2A} ligand [^{11}C]MDL 100907. J Cereb Blood Flow Metab. 2000;20(6):899–909.
24. Talvik-Lotfi M, Nyberg S, Nordstrom AL, Ito H, Halldin C, Brunner F, et al. High 5-HT_{2A} receptor occupancy in MDL 100907 treated schizophrenic patients. Psychopharmacology. 2000;148(4):400–3.
25. Pinborg LH, Adams KH, Svarer C, Holm S, Hasselbalch SG, Haugbol S, et al. Quantification of 5-HT_{2A} receptors in the human brain using [^{18}F]altanserin-PET and the bolus/infusion approach. J Cereb Blood Flow Metab. 2003;23(8):985–96.
26. Talbot PS, Slifstein M, Hwang DR, Huang Y, Scher E, Abi-Dargham A, et al. Extended characterisation of the serotonin 2A (5-HT_{2A}) receptor-selective PET radiotracer [^{11}C]MDL 100907 in humans: quantitative analysis, test-retest reproducibility, and vulnerability to endogenous 5-HT tone. Neuroimage. 2012;59(1):271–85.
27. Meyer PT, Bhagwagar Z, Cowen PJ, Cunningham VJ, Grasby PM, Hinz R. Simplified quantification of 5-HT_{2A} receptors in the human brain with [^{11}C]MDL 100907 PET and non-invasive kinetic analyses. Neuroimage. 2010;50(3):984–93.
28. Hinz R, Bhagwagar Z, Cowen PJ, Cunningham VJ, Grasby PM. Validation of a tracer kinetic model for the quantification of 5-HT_{2A} receptors in human brain with [^{11}C]MDL 100907. J Cereb Blood Flow Metab. 2007;27(1):161–72.
29. Hall H, Farde L, Halldin C, Lundkvist C, Sedvall G. Autoradiographic localization of 5-HT_{2A} receptors in the human brain using [^{3}H]MDL 100907 and [^{11}C]MDL 100907. Synapse. 2000;38(4):421–31.
30. Debus F, Herth MM, Piel M, Buchholz HG, Bausbacher N, Kramer V, et al. ^{18}F-labeling and evaluation of novel MDL 100907 derivatives as potential 5-HT_{2A} antagonists for molecular imaging. Nucl Med Biol. 2010;37(4):487–95.
31. Hansen HD, Ettrup A, Herth MM, Dyssegaard A, Ratner C, Gillings N, et al. Direct comparison of [^{18}F]MH.MZ and [^{18}F]altanserin for 5-HT_{2A} receptor imaging with PET. Synapse. 2013;67(6):328–37.
32. Herth MM, Piel M, Debus F, Schmitt U, Luddens H, Rosch F. Preliminary in vivo and ex vivo evaluation of the 5-HT2A imaging probe [^{18}F]MH.MZ. Nucl Med Biol. 2009;36(4):447–54.
33. Herth MM, Debus F, Piel M, Palner M, Knudsen GM, Luddens H, et al. Total synthesis and evaluation of [^{18}F]MH.MZ. Bioorg Med Chem Lett. 2008;18(4):1515–9.
34. Herth MM, Kramer V, Gillings N, Rösch F, Knudsen GM. Direct radiofluorination of [^{18}F]MH.MZ for 5-HT_{2A} receptor molecular imaging with PET. J Label Compd Radiopharm. 2012;55(9):354–8.
35. Abi-Dargham A, Martinez D, Mawlawi O, Simpson N, Hwang DR, Slifstein M, et al. Measurement of striatal and extrastriatal dopamine D_1 receptor binding potential with [^{11}C]NNC 112 in humans: validation and reproducibility. J Cereb Blood Flow Metab. 2000;20(2):225–43.
36. Gillings N. A restricted access material for rapid analysis of ^{11}C-labeled radiopharmaceuticals and their metabolites in plasma. Nucl Med Biol. 2009;36(8):961–5.
37. Hammers A, Allom R, Koepp MJ, Free SL, Myers R, Lemieux L, et al. Three-dimensional maximum probability atlas of the human brain, with particular reference to the temporal lobe. Hum Brain Mapp. 2003;19(4):224–47.
38. Innis RB, Cunningham VJ, Delforge J, Fujita M, Gjedde A, Gunn RN, et al. Consensus nomenclature for in vivo imaging of reversibly binding radioligands. J Cereb Blood Flow Metab. 2007;27(9):1533–9.
39. Schmidt KC, Turkheimer FE. Kinetic modeling in positron emission tomography. Q J Nucl Med. 2002;46(1):70–85.
40. Pazos A, Cortes R, Palacios JM. Quantitative autoradiographic mapping of serotonin receptors in the rat brain. II. Serotonin-2 receptors. Brain Res. 1985;346(2):231–49.
41. Nishizawa S, Benkelfat C, Young SN, Leyton M, Mzengeza S, de Montigny C, et al. Differences between males and females in rates of serotonin synthesis in human brain. Proc Natl Acad Sci U S A. 1997;94(10):5308–13.

42. Adams KH, Pinborg LH, Svarer C, Hasselbalch SG, Holm S, Haugbol S, et al. A database of [^{18}F]-altanserin binding to 5-HT_{2A} receptors in normal volunteers: normative data and relationship to physiological and demographic variables. Neuroimage. 2004;21(3):1105–13.
43. Horsager J, Munk OL, Sorensen M. Metabolic liver function measured in vivo by dynamic ^{18}F-FDGal PET/CT without arterial blood sampling. EJNMMI Res. 2015;5:32–7.
44. Sadzot B, Lemaire C, Maquet P, Salmon E, Plenevaux A, Degueldre C, et al. Serotonin 5HT2 receptor imaging in the human brain using positron emission tomography and a new radioligand, [^{18}F]altanserin: results in young normal controls. J Cereb Blood Flow Metab. 1995;15(5):787–97.
45. Lundkvist C, Halldin C, Ginovart N, Nyberg S, Swahn CG, Carr AA, et al. [^{11}C]MDL 100907, a radioligland for selective imaging of 5-HT_{2A} receptors with positron emission tomography. Life Sci. 1996;58(10):PL 187–92.